

A visible-light-sensitive siloxene-based composite material with enhanced photocatalytic activity

Hyeo Ji Kang, Sunhye Lee, Hyuk Joon Jung, Hee Jung Yang, Kyu Hyung Lee, Nam Hwi Hur*

Department of Chemistry, Sogang University, 35 Baekbeom-ro, Mapo-gu, Seoul, 04107, Republic of Korea

ARTICLE INFO

Keywords:
Siloxene
Graphene
Composites
Nanosheet
Photocatalyst

ABSTRACT

A novel layer-stacking approach that produces a layered composite of siloxene and reduced graphene oxide (RGO) sheets is presented. This method is based on the assembly of siloxene and graphene oxide sheets, followed by reduction at low temperature using solid hydrazine. High-resolution transmission electron microscopy reveals that the resulting siloxene-RGO composite has a layered structure with sheets that appear to be alternately stacked in a face-to-face fashion. This composite exhibits excellent photocatalytic activity under visible-light irradiation, with a photocurrent density that is about 40 times higher than that of the siloxene sheets alone. It is evident that the RGO sheets stacked on the siloxene surfaces are the key elements that increase the photocatalytic activity of the layered composite. This layer-stacking approach enhances siloxene properties in many ways, rendering ample opportunities for the development of new siloxene-based composite materials with novel functionalities.

1. Introduction

Graphene sheets composed of two dimensional (2D) layers of sp^2 -bonded carbons have unique electronic, optical, and mechanical properties [1–12]. In contrast to pristine graphite, the basal planes of graphene sheets are easily functionalized, which facilitates the preparation of a wide range of graphene-based materials and their utilization in a variety of applications. [13–15] Recent advances in our understanding of graphene sheets has evoked new interest in the ordered planar 2D sheets composed of other moieties such as silicon [16–22], germanium [23–26], boron nitride [27–32], metal carbides [33–37], and metal dichalcogenides and nitrides [38–47].

Siloxene is a layered silicon sheet with a nominal stoichiometry close to $Si_6H_3(OH)_3$, in which the Si atoms in the puckered layer are alternately terminated by hydrogen (H) and hydroxyl (OH) groups [48–51]. Siloxene sheets are typically prepared by immersing calcium silicide ($CaSi_2$) in concentrated HCl solution. The Zintl-type $CaSi_2$ phase is composed of 2D puckered $[Si^-]_2$ layers that are separated from each other by Ca^{2+} cations [52–55]. The cations are removed by Cl^- anions while maintaining the anionic $[Si^-]_2$ structure. The Si atoms in the puckered $[Si^-]_2$ layers are terminated by H- and OH- groups. The terminating groups in siloxene not only make the planar structure stable but also render the siloxene sheet dispersible in water. Unlike bulk silicon, siloxene has a direct band gap, which produces very efficient

photoemission in the visible region [56–59]. A drawback, however, is that the siloxene sheets are not conductive, which limits their electronic and photocatalytic applications. An alternative way of exploiting the 2D properties of siloxene is through the preparation of composites with conductive graphene sheets, such as reduced graphene oxide (RGO). The incorporation of RGO components into the siloxene matrix would improve its conductivity and enhance its mechanical strength.

Here, we report a novel method for the preparation of siloxene-RGO composites via the complete linking of siloxene and graphene oxide (GO) sheets through the use of 3-amino propyl-trimethoxy-silane (APTMS), followed by the solid-state reduction of the linked planar composite with solid hydrazine ($NH_3^+NHCO_2^-$). The siloxene-RGO composite, synthesized by this method, exhibits excellent photoelectrochemical properties and produces high photocurrents under visible-light irradiation compared to the parent siloxene sheets. This layer-by-layer assembly approach enhances the properties of siloxene, rendering ample opportunities for the development of new siloxene-based composite materials with novel functionalities.

2. Materials and methods

2.1. Materials

All chemicals were obtained from commercial suppliers and were

* Corresponding author.

E-mail address: nhhur@sogang.ac.kr (N.H. Hur).

<https://doi.org/10.1016/j.jphotochem.2018.07.026>

Received 2 April 2018; Received in revised form 2 July 2018; Accepted 17 July 2018

Available online 19 July 2018

1010-6030/ © 2018 Elsevier B.V. All rights reserved.

used without further purification. Silicon (powder, 99.999%), 3-aminopropyltrimethoxysilane (APTMS, 97%), graphite (powder, < 20 μm), potassium permanganate (99%), hydrazine monohydrate ($\text{NH}_2\text{NH}_2\cdot\text{H}_2\text{O}$), and ninhydrin (ACS reagent) were purchased from Sigma Aldrich (St. Louis, MO, USA). Sulfuric acid (H_2SO_4), hydrogen peroxide (H_2O_2), and 35% hydrochloric acid (HCl) were purchased from Jin Chemical Pharmaceutical Co (Seoul, Korea). N,N' -dicyclohexylcarbodiimide (DCC, $\geq 99.0\%$) was obtained from Honeywell Research Chemical (Leicestershire, UK). Calcium silicide (CaSi_2 , Kojundo Chemical Laboratory Co) was used as the starting material for the synthesis of siloxene. Solid hydrazine ($\text{H}_3\text{N}^+\text{NHCO}_2^-$) was purchased from FutureChem (Seoul, Korea).

2.2. Synthesis of siloxene sheets

A three-neck round-bottom flask with a magnetic stirring bar was charged with 1.0 g of CaSi_2 in an argon-filled glove box. After moving the flask into a fume hood, the flask was filled with N_2 , after which 100 mL of concentrated HCl (35%) was slowly added under N_2 . The mixture was stirred at room temperature for 10 h. A yellow precipitate gradually formed at the bottom of the flask. The mother liquor was removed by cannulation and the green solid residue was washed several times with water and ethanol to remove CaCl_2 . The resulting solid was dried under vacuum for 4 h to yield 0.63 g of siloxene ($\text{Si}_6\text{H}_3(\text{OH})_3$) sheets.

2.3. Synthesis of graphene oxide (GO) and APTMS-functionalized siloxene sheets

Graphene oxide (GO) was obtained by the oxidation of graphite powder according to a modification of Hummers method. The resulting GO sheets were dried under vacuum at room temperature for 24 h to give a dark-brown powder. Siloxene sheets were functionalized with APTMS as follows. Briefly, 0.5 g of siloxene was dispersed in 15 mL of ethanol and 0.8 mL of APTMS was added to the solution. The dispersion was stirred for 3 h at 40 $^\circ\text{C}$, after which the resulting APTMS-functionalized siloxene sheets were collected by centrifugation, washed with three times ethanol, and dried under vacuum. The presence of APTMS on the siloxene sheet was confirmed by the ninhydrin test.

2.4. Synthesis of siloxene-reduced graphene oxide (RGO) composites

To prepare the siloxene-GO composite, 0.2 g of the APTMS-functionalized siloxene was dispersed in 100 mL of ethanol while 0.065 g of GO was separately dispersed in 50 mL of ethanol. The two dispersions were mixed and stirred for 30 min. DCC (30 mg) was added to the solution, after which it was allowed to react at 70 $^\circ\text{C}$ for 3 h. The resulting dark-green powder was collected by centrifugation, washed three times with ethanol, and dried under vacuum to afford about 0.176 g of the dried siloxene-GO product. The conversion of siloxene-GO into siloxene-RGO was performed in two ways. First, GO and solid hydrazine was reacted in the solid-state as follows. Briefly, siloxene-GO (0.2 g) was mixed with solid hydrazine (0.1 g) and the mixture was ground using a mortar and pestle in a nitrogen-filled glove box. The ground powder was placed in a 50 mL-glass pressure bottle and allowed to react at 80 $^\circ\text{C}$ for 1 h. The second method is based on the conventional solid-state reaction, in which the siloxene-RGO composite was prepared by annealing the siloxene-GO sample at 300 $^\circ\text{C}$ under Ar/H_2 for 3 h.

2.5. Characterization

Powder X-ray diffraction (XRD) measurements were performed on a Rigaku DMAX 2500 diffractometer (Rigaku, Japan) with $\text{Cu K}\alpha$ radiation ($\lambda = 1.5406 \text{ \AA}$) operating at 40 kV and 150 mA. High-resolution transmission electron microscopy (HRTEM) was performed on a JEOL JEM-2100 F microscope (JEOL, Japan). The HRTEM specimens were

prepared by dispersing finely ground sample powders in anhydrous ethanol. A drop of the suspension was allowed to evaporate on a carbon-coated grid. High-resolution scanning electron microscopy analyses were carried out using a Hitachi S-5500 microscope (Hitachi, Japan). The SEM samples were prepared by dropping diluted samples in anhydrous ethanol on a lacey support grid. Samples were also chemically micro-analyzed using an INCA TEM 300 system (Oxford Instruments, Abingdon, UK) for energy dispersive X-ray (EDX) analysis. UV-vis absorption spectra were recorded using a Lambda 950 spectrophotometer (Perkin Elmer, USA). Powder spectra were recorded by the diffuse reflectance method using an integrating-sphere accessory. Thermogravimetric analysis was carried out using a TGA 2050 instrument (TA Instruments, USA). Samples were placed on a platinum pan and analyzed under nitrogen from 25 to 700 $^\circ\text{C}$ at a heating rate of 10 $^\circ\text{C}/\text{min}$. Raman spectra were obtained using a Jobin-Yvon Triax 550 spectrometer equipped with a liquid-nitrogen-cooled charge-coupled-device detector. The Fourier transform infrared (FT-IR) spectra were measured on a Nicolet 205 FT-IR spectrometer in a KBr pellet, scanning from 4000 to 600 cm^{-1} at room temperature.

2.6. Photoelectrochemical testing

A potentiostat/galvanostat (Model 263 A, Princeton Applied Research, USA) was used for the electrochemical experiments. Before preparation of the working electrode, the indium tin oxide (ITO) glass substrate was cleaned by sonication in ethanol and then acetone for 30 min, after which it was rinsed with distilled water and stored in isopropyl alcohol for 12 h. The composite sample (5 mg) was typically dispersed in 200 μL of dilute Nafion (0.5 wt%) in methanol, after which it was drop-casted onto a 1.0 cm^2 ITO glass substrate. The resulting electrode was dried in air at 100 $^\circ\text{C}$. Photoelectrochemical experiments were performed in a three-electrode cell system with Pt wire as the counter electrode, a Ag/AgCl electrode (3 M NaCl) as the reference electrode, and the sample-coated ITO glass as the working electrode. The three-electrode cell was immersed in a 15-mL Pyrex vial. A 300 W Xe arc lamp with a 420 nm cut-off filter was used as the source of visible light. The working electrodes were illuminated from the rear.

3. Results and discussion

Siloxene sheets were prepared by the HCl-promoted deintercalation of the Ca in CaSi_2 at room temperature, which is schematically illustrated in Fig. 1. After treatment with concentrated HCl for 10 h, the product was collected by filtration, washed with water and then ethanol to remove residual CaCl_2 , followed by drying in vacuo. The color changed from black, in the original CaSi_2 , to yellow in the dried solid, indicating that CaSi_2 has been converted into siloxene by HCl.

The siloxene prepared in this manner was examined by powder X-ray diffraction (XRD), as shown in Fig. 2. New reflections corresponding to siloxene are evident in the XRD profile of this material, which are well indexed to its hexagonal graphitic-like structure, with $a = 3.74 \text{ \AA}$ and $c = 6.44 \text{ \AA}$ [60–62]. They confirm the formation of siloxene with the nominal $\text{Si}_6\text{H}_3(\text{OH})_3$ composition. The broad peaks indicate that the formed siloxene is composed of numerous nanometer-scale siloxene sheets.

A typical high-resolution TEM image and elemental maps of the siloxene sheets are displayed in Fig. 3. The TEM image highlights the planar structure of this material, which is composed of a few-layered sheets, and is consistent with the corresponding XRD data provided in Fig. 1(b). This microstructural TEM image is analogous to that of individual RGO sheets obtained by the reduction of GO [63–65]. The elemental maps confirm the presence of Si and O. The Si image is very distinctive due to the strong scattering power of Si. On the other hand, the O map is blurred mainly because the scattering intensity of oxygen is relatively weak. These maps reveal that Si and O are evenly dispersed over the siloxene surface. Another notable feature is the sparseness of

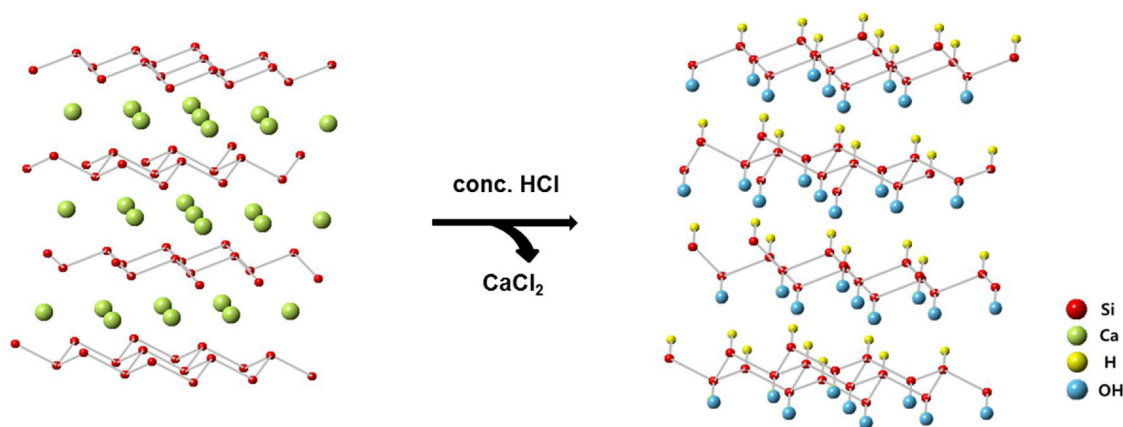


Fig. 1. Schematic illustration of the deintercalation of CaSi_2 at room temperature during the formation of $\text{Si}_6\text{H}_3(\text{OH})_3$ in the presence of HCl (Ca, green; Si, red; H, yellow; OH, blue). (For interpretation of the references to color in this figure legend, the reader is referred to the web version of this article.)

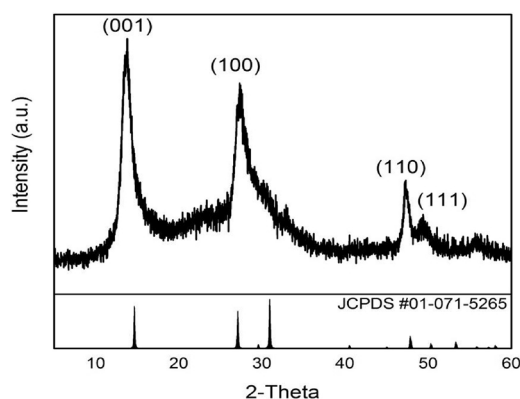


Fig. 2. Powder XRD profiles of $\text{Si}_6\text{H}_3(\text{OH})_3$ obtained following deintercalation of CaSi_2 in the presence of HCl.

the Ca signals on the surface, which suggests that Ca is almost completely deintercalated from the pristine CaSi_2 .

The siloxene sheets were further examined by thermal gravimetric analysis (TGA) and UV–vis spectroscopy. Fig. S1 reveals that the weight percentage of the siloxene sheets increases to about 142% over the original weight upon heating, which is slightly lower than the theoretical value (162%) for complete conversion of $\text{Si}_6\text{H}_3(\text{OH})_3$ into SiO_2 . This suggests that the siloxene sheets might contain partially oxidized SiO_x impurities. The diffuse reflectance UV–vis spectrum of siloxene exhibits an absorption edge near 515 nm (Fig. S2), clearly indicating that the siloxene sheets absorb visible-light. Using the spectral data and the Tauc model [66,67], the optical band gap of the siloxene sheets was estimated to be about 2.4 eV. The band gap energy calculated from the spectral data is slightly larger than the theoretical value (2.2 eV) obtained from local-density-approximation calculations and self-energy corrections [68].

Our initial evaluation of the photocatalytic activity involved investigating the ability of the siloxene sheets to produce photocurrent upon exposure to visible-light. These experiments were conducted in a three-electrode configuration, in which Pt wire was used as the counter electrode, a Ag/AgCl electrode was used as the reference electrode, and catalyst-coated indium tin oxide (ITO) glass was used as the working electrode.

Fig. 4(a) reveals that the siloxene sheets generate photocurrent during repeated cycles of periodic exposure to visible-light; the measured photocurrent density was about $0.15 \mu\text{A}/\text{cm}^2$. Although the current density is larger than that of polycrystalline silicon powder (Fig. S3), it is nevertheless desirable to prepare new composites based on siloxene sheets with further enhanced photocatalytic properties.

One plausible route for enhancing the properties of siloxene for broader applicability involves the preparation of a composite material with conductive graphene sheets. For this reason, we initially focused on the synthesis of individual graphene oxide (GO) sheets, which were prepared by the method reported by Hummers [69–72]. The GO sheets are not yet reduced and are therefore not conductive, but they disperse well in water. This dispersibility facilitates the ready combination of the GO and siloxene sheets, and enables the formation of siloxene-GO composites. We used APTMS as a linker molecule mainly because it is easily anchored onto the hydroxylated siloxene surfaces to provide the required spacing [73–75].

Fig. 5 displays a schematic illustration of the assembly of a GO sheet on an APTMS-functionalized siloxene sheet. The APTMS-functionalized siloxene sheets were first prepared by the condensations of APTMS molecules with the hydroxyl (–OH) groups of the siloxene. The attachment of APTMS onto the siloxene was confirmed by the ninhydrin test. When the APTMS-functionalized siloxene sheet was treated with ninhydrin solution, it turned purple (Fig. S4). The APTMS-functionalized siloxene and GO sheets were then coupled through the formation of amide bonds by the action of di-cyclohexyl-carbodiimide (DCC). A dispersion of GO in water was added into the APTMS-functionalized siloxene solution in the presence of DCC and allowed to react at 70°C for 3 h. The resulting dark-green sheets were separated from the solution by centrifugation and washed with absolute ethanol, followed by drying under vacuum. Elemental maps of the as-prepared siloxene-GO composite clearly reveal even distribution of Si, C, and O elements, as shown in Fig. 4(c), which implies that siloxene and GO sheets are approximately face-to-face stacked.

The siloxene-GO composite was reduced to make it conductive and rigid. A conventional annealing method was initially used to prepare the siloxene-RGO composite, in which annealing was performed at 300°C under an Ar/H_2 atmosphere. As a new low-temperature procedure, solid hydrazine was used to convert GO into RGO without any microstructural changes. The solid-state reaction of hydrazine turns out to be very effective for the reduction of GO. Briefly, this synthesis was accomplished by grinding solid hydrazine with the siloxene-GO composite. The mixed powder was then stored at 80°C for 1 h. A color change to brownish black was noticed during the reaction. The powder XRD profile of the resulting composite clearly reveals that the siloxene-GO composite has been converted into the siloxene-RGO composite (Fig. S5). Broad reflections corresponding to graphitic carbon are observed in the XRD profile of the reduced material, which provides direct evidence for the conversion of GO into RGO [76–78].

The siloxene-RGO composites, prepared by annealing under Ar/H_2 or with solid hydrazine, were further examined by TGA, transmission electron microscopy (TEM), and photocurrent experiments, which confirm that highly conductive siloxene-RGO composites with planar

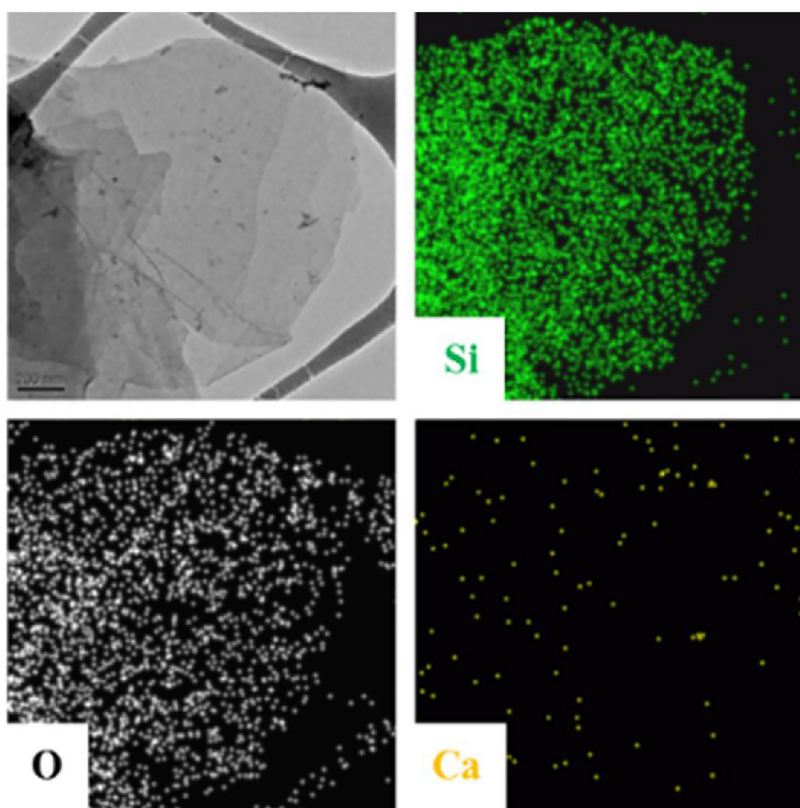


Fig. 3. High-resolution TEM image and elemental maps of freestanding siloxene sheets obtained following the deintercalation of Ca from CaSi_2 . Si (green), O (white), and Ca (yellow) elemental maps of the region within the TEM image. (For interpretation of the references to color in this figure legend, the reader is referred to the web version of this article.)

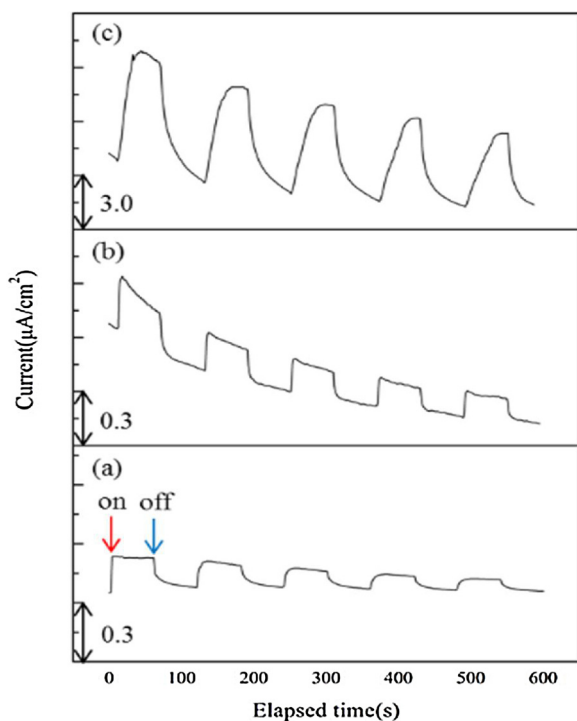


Fig. 4. Photocurrent responses of (a) siloxene sheets, (b) the siloxene-RGO composite prepared by annealing under Ar/H_2 , and (c) the siloxene-RGO composite obtained by reduction with solid hydrazine. The data were collected at an applied potential of 0.8 V (versus Ag/AgCl) with periodic visible-light irradiation.

geometries were formed. As illustrated in Fig. S6, the weight percentage of the siloxene-RGO composite obtained by solid hydrazine reduction gradually decreased to about 89% of its initial value at 700 °C, which is

about the same as that observed for freestanding RGO sheets. A similar weight-change trend was observed for the siloxene-RGO composite prepared by annealing under Ar/H_2 , as revealed by TGA. The TGA data also suggest that GO sheets in both composites were completely converted into RGO sheets.

We employed Raman spectroscopy to further evaluate the siloxene-RGO composite. The spectrum, given in Fig. S7, shows two peaks at 1357 and 1590 cm^{-1} , which correspond to D and G bands, respectively. Besides the D and G peaks, a sharp peak appears at 521 cm^{-1} , which corresponds to the Si-Si band. The siloxene-RGO composite was also characterized by FT-IR to analyze the linkage between the siloxene and RGO sheets (See Fig. S8). For comparison, we included IR spectra of the GO, siloxene, and siloxene-GO samples. After the reduction finished with solid hydrazine, almost all the peaks of the oxygen-containing species such as hydroxyl (C–OH), ketonic species (C=O), carboxyl (COOH), and epoxide (C–O–C) species vanished while the peak at 1080 cm^{-1} responsible for Si–O–Si stretching retained. The Raman and IR data suggest that the RGO sheets are connected to the siloxene sheets.

The surface morphologies of the siloxene-RGO composites are directly associated with enhanced electrical and mechanical properties, which were examined by TEM. Fig. 6 displays elemental Si, C and O maps of the two composites, which reveal that all three elemental signals in the composite obtained by solid hydrazine reduction are evenly dispersed, suggesting that the stacking mode of the parent siloxene-GO composite is retained even after reduction. Presumably the low reduction temperature is responsible for the preservation of the parent structure. The solid-state reduction method provides a very effective approach for reducing GO-based composites. In contrast, the composite prepared by annealing at 300 °C exhibits an uneven distribution of C signals over the same region. The RGO sheets formed by annealing appear to be folded, suggesting that the high-temperature annealing partially agglomerates the graphene sheets.

Fig. 4(c) reveals that the photocurrent density of the siloxene-RGO composite obtained using solid hydrazine is about 40 times higher than

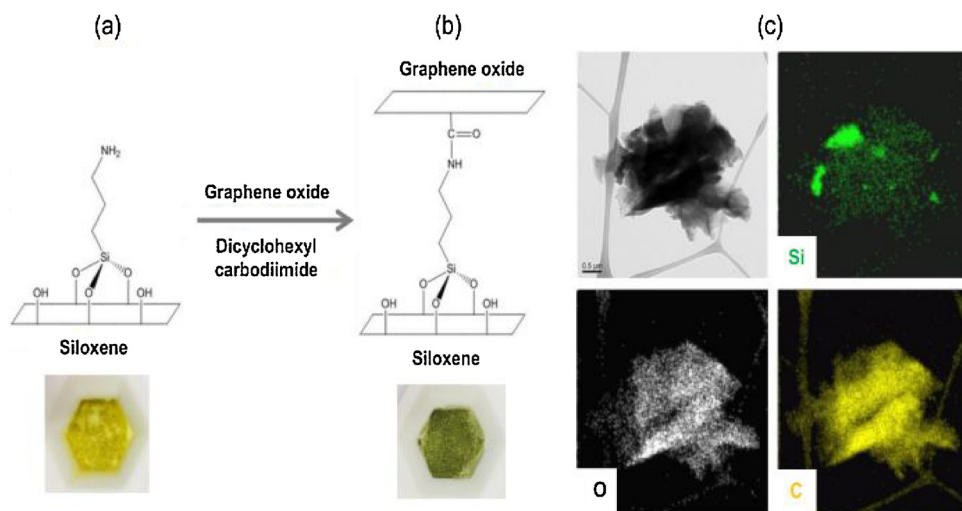


Fig. 5. Schematic diagram proposed for the assembly of a GO sheet on an APTMS-functionalized siloxene sheet. (a) A hydroxylated surface functionalized by APTMS and (b) assembly of a GO sheet on an APTMS-functionalized siloxene sheet. (c) TEM image and elemental maps of the siloxene-GO composite. The bottoms of panels of (a) and (b) show photographic images of the powders corresponding to the depicted sheet structures.

that of the siloxene sheets alone. Such a large enhancement is probably attributable to the even attachment of the conductive RGO sheets across the siloxene surface. In other words, the reduction of GO in the absence of a solvent prevents the aggregation of RGO sheets and maintains the face-to-face stacked structure of the siloxene and RGO sheets. In contrast, a very slight enhancement in photocurrent density was also observed for the siloxene-RGO composite prepared by annealing under an Ar/H₂ atmosphere, although it is not as large as the composite prepared by solid hydrazine reduction. This indicates that the use of GO sheets for the preparation of these composites is not the sole reason for the observed increase in current density; the sheet-stacking quality also appears to be crucial for achieving excellent photocatalytic activity.

4. Conclusions

In conclusion, we successfully synthesized a new siloxene-RGO composite by the controlled linking of GO sheets to siloxene and subsequent reduction using solid hydrazine. The siloxene-RGO composite comprises multiple-layered sheets and exhibits high photocatalytic activity under visible-light irradiation. The origin of the enhanced activity

is presumably due to the conductive nature of RGO and the layer-by-layer assembly of the siloxene and RGO sheets. We anticipate that our low-temperature chemical strategy for the preparation of composites comprising siloxene and RGO sheets will lead to the development of a wide range of 2D materials with new functionalities and enhanced properties.

Acknowledgments

This work was supported by “Human Resources Program in Energy Technology” of the Korea Institute of Energy Technology Evaluation and Planning (KETEP), and financially supported by the Ministry of Trade, Industry & Energy, Republic of Korea (No. 20174010201150). This research was supported by Basic Science Research Program through the National Research Foundation Korea (NRF) funded by the Ministry of Education (NRF-2017R1A6A3A11031777) K.H.L. thanks the Research Institute for Basic Science in Sogang University.

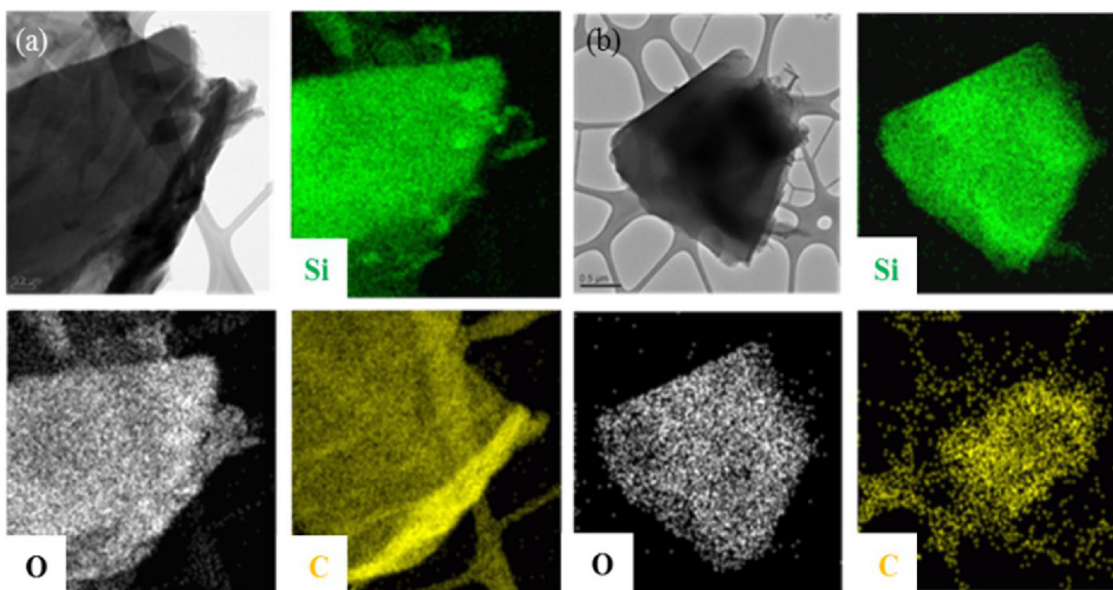


Fig. 6. TEM images and elemental maps of the siloxene-RGO composites (a) obtained by reduction with solid hydrazine and (b) prepared by annealing under Ar/H₂. Si (green), O (white), and C (yellow) elemental maps of the regions within the TEM images. (For interpretation of the references to color in this figure legend, the reader is referred to the web version of this article.)

Appendix A. Supplementary data

Supplementary material related to this article can be found, in the online version, at doi:<https://doi.org/10.1016/j.jphotochem.2018.07.026>.

References

- [1] S. Butler, S.M. Hollen, L.Y. Cao, Y. Cui, J.A. Gupta, H.R. Gutierrez, T.F. Heinz, S.S. Hong, J.X. Huang, A.F. Ismach, E. Johnston-Halperin, M. Kuno, V.V. Plashnitsa, R.D. Robinson, R. Ruoff, S. Salahuddin, J. Shan, L. Shi, M.G. Spencer, M. Terrones, W. Windl, J.E. Goldberger, Progress, challenges, and opportunities in two-dimensional materials beyond graphene, *ACS Nano* 7 (2013) 2898–2926.
- [2] A. Geim, K. Novoselov, The rise of graphene, *Nat. Mater.* 6 (2007) 183–191.
- [3] A. Balandin, Thermal properties of graphene and nanostructured carbon materials, *Nat. Mater.* 10 (2011) 569–581.
- [4] D. Chen, H. Feng, J. Li, Graphene oxide: preparation, functionalization, and electrochemical applications, *Chem. Rev.* 112 (2012) 6027–6053.
- [5] C. Chua, M. Pumer, Covalent chemistry on graphene, *Chem. Soc. Rev.* 42 (2013) 3222–3233.
- [6] N. Morimoto, T. Kubo, Y. Nishina, Tailoring the oxygen content of graphite and reduced graphene oxide for specific applications, *Sci. Rep.* 6 (2016) 21715–21723.
- [7] D.R. Dreyer, S. Park, C. Bielawski, R. Ruoff, The chemistry of graphene oxide, *Chem. Soc. Rev.* 39 (2010) 228–240.
- [8] S. Bae, H. Kim, Y. Lee, X.F. Xu, J.S. Park, Y. Zheng, J. Balakrishnan, T. Lei, H.R. Kim, Y.I. Song, Y.J. Kim, K.S. Kim, B. Ozyilmaz, J.H. Ahn, B.H. Hong, S. Iijima, Roll-to-roll production of 30-inch graphene films for transparent electrodes, *Nat. Nanotechnol.* 5 (2010) 574–578.
- [9] P. Avouris, Graphene: electronic and photonic properties and devices, *Nano Lett.* 10 (2010) 4285–4294.
- [10] V. Nicolosi, M. Chhowalla, M.G. Kanatzidis, M.S. Strano, J.N. Coleman, Liquid exfoliation of layered materials, *Science* 340 (2013) 1420.
- [11] H. Kim, Y. Kim, T. Kim, A.R. Jang, H.Y. Jeong, S.H. Han, D.H. Yoon, H.S. Shin, D.J. Bae, K.S. Kim, W.S. Yang, Enhanced optical response of hybridized VO₂/graphene films, *Nanoscale* 5 (2013) 2632–2636.
- [12] M. Marchena, Z. Song, W. Senaratne, C.N. Li, X.Y. Liu, D. Baker, J.C. Ferrer, P. Mazumder, K. Soni, R. Lee, V. Pruneri, Direct growth of 2D and 3D graphene nano-structures over large glass substrates by tuning a sacrificial Cu-template layer, *2D Mater.* 4 (2017).
- [13] S. Wang, L. Yang, Q. Wang, Y. Fan, J. Shang, S. Qiu, J. Li, W. Zhang, X. Wu, Supramolecular self-assembly of layer-by-layer graphene film driven by the synergism of π - π and hydrogen bonding interaction, *J. Photochem. Photobiol. A* 355 (2018) 249–255.
- [14] F. Li, X. Jiang, J. Zhano, S. Zhang, Graphene oxide: a promising nanomaterial for energy and environmental applications, *Nano Energy* 16 (2015) 488–515.
- [15] W. Tie, S.S. Bhattacharyya, Y. Wang, W. He, S.H. Lee, Facile in-situ synthesis of a zinc oxide crystals/few-layered graphene flake composite for enhanced photocatalytic performance, *J. Photochem. Photobiol. A* 348 (2017) 89–95.
- [16] H. Okamoto, Y. Sugiyama, H. Nakano, Synthesis and modification of silicon nanosheets and other silicon nanomaterials, *Chem.-Eur. J.* 17 (2011) 9864–9887.
- [17] K. Koski, Y. Cui, The new skinny in two-dimensional nanomaterials, *ACS Nano* 7 (2013) 3739–3743.
- [18] S. Yamanaka, Silicon clathrates and carbon analogs: high pressure synthesis, structure, and superconductivity, *Dalton Trans.* 39 (2010) 1901–1915.
- [19] J. Ohshita, K. Yamamoto, D. Tanaka, M. Nakashima, Y. Kunugi, M. Ohashi, H. Nakano, Preparation and photocurrent generation of silicon nanosheets with aromatic substituents on the surface, *J. Phys. Chem. C* 120 (2016) 10991–10996.
- [20] Y. Kumai, H. Kadoura, E. Sudo, M. Iwaki, H. Okamoto, Y. Sugiyama, H. Nakano, Si-C composite anode of layered polysilane (Si₄H₆) and sucrose for lithium ion rechargeable batteries, *J. Mater. Chem.* 21 (2011) 11941–11946.
- [21] L. Sun, T. Su, L. Xu, M. Liu, H. Du, Two-dimensional ultra-thin SiOx (0 < x < 2) nanosheets with long-term cycling stability as lithium ion battery anodes, *Chem. Commun.* 52 (2016) 4341–4344.
- [22] M. Ohashi, H. Nakano, T. Morishita, M.J.S. Spencer, Y. Ikemoto, C. Yogi, T. Ohta, Mechanochemical lithiation of layered polysilane, *Chem. Commun.* 50 (2014) 9761–9764.
- [23] E. Bianco, S. Butler, S.S. Jiang, O.D. Restrepo, W. Windl, J.E. Goldberger, Stability and exfoliation of germanane: a germanium graphene analogue, *ACS Nano* 7 (2013) 4414–4421.
- [24] A. Atsalakis, L. Tsetseris, First-principles study of siloxene and germoxene: stable conformations, electronic properties, and defects, *J. Phys.-Condens. Mat.* 26 (2014).
- [25] J. Young, B. Chitara, N. Cultrara, M. Arguilla, S. Jiang, F. Fan, E. Johnston-Halperin, J.E. Goldberger, Water activated doping and transport in multilayered germanane crystals, *J. Phys.-Condens. Mat.* 28 (2016).
- [26] S. Jiang, S. Butler, E. Bianco, O.D. Restrepo, W. Windl, J.E. Goldberger, Improving the stability and optical properties of germanane via one-step covalent methylation, *Nat. Commun.* 5 (2014) 3389.
- [27] Y. Lin, T. Williams, J. Connell, Soluble, exfoliated hexagonal boron nitride nanosheets, *J. Phys. Chem. Lett.* 1 (2010) 277–283.
- [28] S. Yuan, B. Toury, C. Journet, A. Brioude, Synthesis of hexagonal boron nitride graphene-like few layers, *Nanoscale* 6 (2014) 7838–7841.
- [29] J. Wu, L. Yin, L. Zhang, Tuning the electronic structure, bandgap energy and photoluminescence properties of hexagonal boron nitride nanosheets via a controllable Ce³⁺ ions doping, *RSC Adv.* 3 (2013) 7408–7418.
- [30] C.Y. Zhi, Y. Bando, C.C. Tang, H. Kuwahara, D. Golberg, Large-scale fabrication of boron nitride nanosheets and their utilization in polymeric composites with improved thermal and mechanical properties, *Adv. Mater.* 21 (2009) 2889–2893.
- [31] C. Su, W. Chu, Z. Juang, K. Chen, B. Cheng, F. Chen, K. Leou, C. Tsai, Large-scale synthesis of boron nitride nanotubes with iron-supported catalysts, *J. Phys. Chem. C* 113 (2009) 14732–14738.
- [32] J. Coleman, M. Lotya, A. O'Neill, S.D. Bergin, P.J. King, U. Khan, K. Young, A. Gaucher, S. De, R.J. Smith, I.V. Shvets, S.K. Arora, G. Stanton, H.Y. Kim, K. Lee, G.T. Kim, G.S. Duesberg, T. Hallam, J.J. Boland, J. Wang, J.F. Donegan, J.C. Grunlan, G. Moriarty, A. Shmeliov, R.J. Nicholls, J.M. Perkins, E.M. Grievson, K. Theuwissen, D.W. McComb, P.D. Nellist, V. Nicolosi, Two-dimensional nanosheets produced by liquid exfoliation of layered materials, *Science* 331 (2011) 568–571.
- [33] B. Anasori, M.R. Lukatskaya, Y. Gogotsi, 2D metal carbides and nitrides (MXenes) for energy storage, *Nat. Rev. Mater.* 2 (2017) 16098.
- [34] J. Lei, X. Zhang, Z. Zhou, Recent advances in MXene: preparation, properties, and applications, *Front. Phys.-Beijing.* 10 (2015) 276–286.
- [35] P. Urbankowski, B. Anasori, T. Makaryan, D.Q. Er, S. Kota, P.L. Walsh, M.Q. Zhao, V.B. Shenoy, M.W. Barsoum, Y. Gogotsi, Synthesis of two-dimensional titanium nitride Ti₄N₃ (MXene), *Nanoscale* 8 (2016) 11385–11391.
- [36] M. Naguib, M. Kurtoglu, V. Presser, J. Lu, J.J. Niu, M. Heon, L. Hultman, Y. Gogotsi, M.W. Barsoum, Two-dimensional nanocrystals produced by exfoliation of Ti₃AlC₂, *Adv. Mater.* 23 (2011) 4248–4253.
- [37] P. Eklund, J. Rosen, P.O.A. Persson, Layered ternary M_(n+1)AX_n phases and their 2D derivative MXene: an overview from a thin-film perspective, *J. Phys. D: Appl. Phys.* 50 (2017) 113001.
- [38] S. Manzeli, D. Ovchinnikov, D. Pasquier, O.V. Yazyev, A. Kis, 2D transition metal dichalcogenides, *Nat. Rev. Mater.* 2 (2017) 17033.
- [39] R. Lv, J.A. Robinson, R.E. Schaak, D. Sun, Y.F. Sun, T.E. Mallouk, M. Terrones, Transition metal dichalcogenides and beyond: synthesis, properties, and applications of single- and few-layer nanosheets, *Acc. Chem. Res.* 48 (2015) 56–64.
- [40] M. Chhowalla, Z. Liu, H. Zhang, Two-dimensional transition metal dichalcogenide (TMD) nanosheets, *Chem. Soc. Rev.* 44 (2015) 2584–2586.
- [41] Y. Shi, H. Li, L. Li, Recent advances in controlled synthesis of two-dimensional transition metal dichalcogenides via vapour deposition techniques, *Chem. Soc. Rev.* 44 (2015) 2744–2756.
- [42] A. Eftekhari, Tungsten dichalcogenides (WS₂, WSe₂, and WTe₂): materials chemistry and applications, *J. Mater. Chem. A* 5 (1) (2017) 8299–18325.
- [43] J. Yang, H.S. Shin, Recent advances in layered transition metal dichalcogenides for hydrogen evolution reaction, *J. Mater. Chem. A* 2 (2014) 5979–5985.
- [44] J. Xie, J. Xin, G. Cui, X. Zhang, L. Zhou, Y. Wang, W. Liu, C. Wang, M. Ning, X. Xia, Y. Zhao, Vertically aligned oxygen-doped molybdenum disulfide nanosheets grown on carbon cloth realizing robust hydrogen evolution reaction, *Inorg. Chem. Front.* 3 (2016) 1160–1166.
- [45] J. Xie, R. Wang, J. Bao, X. Zhang, H. Zhang, S. Li, Y. Xie, Zirconium trisulfide ultrathin nanosheets as efficient catalysts for water oxidation in both alkaline and neutral solutions, *Inorg. Chem. Front.* 1 (2014) 751–756.
- [46] J. Xie, Y. Xie, Transition metal nitrides for electrocatalytic energy conversion: opportunities and challenges, *Chem. Eur. J.* 22 (2016) 3588–3598.
- [47] J. Xie, Y. Xie, Structural engineering of electrocatalysts for the hydrogen evolution reaction: order or disorder? *ChemCatChem* 7 (2015) 2568–2580.
- [48] H. Nakano, M. Ishii, H. Nakamura, Preparation and structure of novel siloxene nanosheets, *Chem. Commun.* (2005) 2945–2947.
- [49] H. Nakano, Synthesis and modification of two-dimensional crystalline silicon nanosheets, *J. Ceram. Soc. Jpn.* 122 (2014) 748–754.
- [50] H. Fuchs, M. Stutzmann, M. Brandt, M. Rosenbauer, J. Weber, A. Breitschwerdt, P. Deak, M. Cardona, Porous silicon and siloxene - vibrational and structural-properties, *Phys. Rev. B* 48 (1993) 8172–8183.
- [51] F. Kenny, R. Kurtz, Siloxene as chemiluminescent indicator in titration, *Anal. Chem.* 22 (1950) 693–697.
- [52] H. Nakano, T. Ikuno, Soft chemical synthesis of silicon nanosheets and their applications, *Phys. Rev. B* 3 (2016) 40803.
- [53] S. Yamanaka, H. Matsuura, M. Ishikawa, New deintercalation reaction of calcium from calcium disilicide. Synthesis of layered polysilane, *Mater. Res. Bull.* 31 (1996) 307–316.
- [54] H. Nakano, T. Mitsuoka, M. Harada, K. Horibuchi, H. Nozaki, N. Takahashi, T. Nonaka, Y. Seno, H. Nakamura, Soft synthesis of single-crystal silicon monolayer sheets, *Angew. Chem. Int. Ed.* 45 (2006) 6303–6306.
- [55] A. Lyuleeva, T. Helbich, B. Rieger, P. Lugli, Polymer-silicon nanosheet composites: bridging the way to optoelectronic applications, *J. Phys. D: Appl. Phys.* 50 (2017) 135106.
- [56] S. Li, H. Wang, D. Li, X. Zhang, Y. Wang, J. Xie, J. Wang, Y. Tian, W. Ni, Y. Xie, Siloxene nanosheets: a metal-free semiconductor for water splitting, *J. Mater. Chem. A* 4 (2016) 15841–15844.
- [57] H. Itahara, H. Nakano, Synthesis and optical properties of two-dimensional silicon compounds, *Jpn. J. Appl. Phys.* 56 (2017) 05DA02.
- [58] Y. Sugiyama, H. Okamoto, T. Mitsuoka, T. Morikawa, K. Nakanishi, T. Ohta, H. Nakano, Synthesis and optical properties of monolayer organosilicon nanosheets, *J. Am. Chem. Soc.* 132 (2010) 5946–5947.
- [59] H. Itahara, X. Wu, H. Imagawa, S. Yin, K. Kojima, S. Chichibu, T. Sato, Photocatalytic activity of silicon-based nanoflakes for the decomposition of nitrogen monoxide, *Dalton Trans.* 46 (2017) 8643–8648.
- [60] Y. Sugiyama, H. Okamoto, H. Nakano, Synthesis of siloxene derivatives with organic groups, *Chem. Lett.* 39 (2010) 938–939.
- [61] A. Weiss, G. Beil, H. Meyer, The topochemical reaction of CaSi₂ to a two-dimensional

- subsiliceous acid $\text{Si}_6\text{H}_3(\text{OH})_3$ (Kautskys' Siloxene), *Naturforsch. B* 35 (1979) 25–30.
- [62] J. Dahn, B. Way, E. Fuller, J. Tse, Structure of siloxene and layered polysilane (Si_6H_6), *Phys. Rev. B* 48 (1993) 17872–17877.
- [63] X. Luo, X. Wang, S. Bao, X. Liu, W. Zhang, T. Fang, Adsorption of phosphate in water using one-step synthesized zirconium-loaded reduced graphene oxide, *Sci. Rep.* 6 (2016) 39108.
- [64] L. He, R. Ma, N. Du, J. Ren, T. Wong, Y. Li, S. Lee, Growth of TiO_2 nanorod arrays on reduced graphene oxide with enhanced lithium-ion storage, *J. Mater. Chem.* 22 (2012) 19061–19066.
- [65] J. Lu, Y. Li, S. Li, S. Jiang, Self-assembled platinum nanoparticles on sulfonic acid-grafted graphene as effective electrocatalysts for methanol oxidation in direct methanol fuel cells, *Sci. Rep.* 6 (2016) 21530.
- [66] J. Tauc, R. Grigorovici, A. Vancu, Optical properties and electronic structure of amorphous germanium, *Phys. Status Solidi* 15 (15) (1966) 627–637.
- [67] B. Viezbicke, S. Patel, B. Davis, D. Birnie, Evaluation of the Tauc method for optical absorption edge determination: ZnO thin films as a model system, *Phys. Status Solidi B* 252 (2015) 1700–1710.
- [68] K. Takeda, K. Shiraishi, Electronic-structure of silicon-oxygen high polymers, *Solid State Commun.* 85 (1993) 301–305.
- [69] W. Hummers, R. Offeman, Preparation of graphitic oxide, *J. Am. Chem. Soc.* 80 (1958) 1339.
- [70] H. Yu, B. Zhang, C. Bulin, R. Li, R. Xing, High-efficient synthesis of graphene oxide based on improved hummers method, *Sci. Rep.* 6 (2016) 36143.
- [71] J. Park, Y.S. Kim, S.J. Sung, T. Kim, C.R. Park, Highly dispersible edge-selectively oxidized graphene with improved electrical performance, *Nanoscale* 9 (2017) 1699–1708.
- [72] J. Qu, F. Gao, Q. Zhou, Z. Wang, H. Hu, B. Li, W. Wan, X. Wang, J. Qiu, Highly atom-economic synthesis of graphene/ Mn_2O_4 hybrid composites for electrochemical supercapacitors, *Nanoscale* 5 (2013) 2999–3005.
- [73] J. Hicks, R. Dabestani, A. Buchanan, C. Jones, Spacing and site isolation of amine groups in 3-aminopropyl-grafted silica materials: the role of protecting groups, *Chem. Mater.* 18 (2006) 5022–5032.
- [74] P.C. Pandey, S. Shukla, Y. Pandey, 3-Aminopropyltrimethoxysilane and graphene oxide/reduced graphene oxide-induced generation of gold nanoparticles and their nanocomposites: electrocatalytic and kinetic activity, *RSC Adv.* 6 (2016) 80549–80556.
- [75] F. Zhang, S. Lv, J. Jiang, Y. Ni, Preparation of siloxene nanosheet-supported palladium as sustainable catalyst for Mizoroki-Heck reaction, *Appl. Organomet. Chem.* 28 (2014) 826–830.
- [76] M. Khandelwal, A. Kumar, One-step chemically controlled wet synthesis of graphene nanoribbons from graphene oxide for high performance supercapacitor applications, *J. Mater. Chem. A* 3 (2015) 22975–22988.
- [77] G. Liu, L. Wang, B. Wang, T. Gao, D. Wang, A reduced graphene oxide modified metallic cobalt composite with superior electrochemical performance for supercapacitors, *RSC Adv.* 5 (2015) 63553–63560.
- [78] Z. Feng, C. Zhang, J. Chen, Y. Wang, X. Jin, R. Zhang, J. Hu, An easy and eco-friendly method to prepare reduced graphene oxide with $\text{Fe}(\text{OH})_2$ for use as a conductive additive for LiFePO_4 cathode materials, *RSC Adv.* 3 (2013) 4408–4415.